



Optimizing volume estimation in aquaculture sea cages: A comparative study of calculation methods and sensor placement

Heðin I. Abrahamsen^{a,c,*}, Tróndur T. Johannesen^a, Øystein Patursson^b, Knud Simonsen^c

^a Firum, við Áir 11, Hvalvík, FO 430, Faroe Islands

^b RAO SP/F, í Geilini 11, Kirkjubøur, FO 175, Faroe Islands

^c University of the Faroe Islands, Faculty of Science and Technology, Vestara Bryggja, Tórshavn, FO 100, Faroe Islands

ARTICLE INFO

Dataset link: <https://doi.org/10.5281/zenodo.10202190>

Keywords:

Aquaculture
Exposed areas
Volume calculation
Pressure sensors
Waves and currents
Cage deformation

ABSTRACT

Due to intensified environmental challenges and industry growth, salmon aquaculture is expanding into regions with stronger currents and higher waves. This can expose sea cages to the elements and result in pronounced cage deformations. Such deformations diminish net volume, potentially jeopardizing fish welfare and survival. A prevalent approach to gauging these deformations involves attaching pressure sensors at strategic locations on the cage. This study presents a comprehensive analysis of methods for calculating the volume of deformed aquaculture cages, categorizing them into two main approaches. The first approach involves dividing the cage's surface into triangular sections to calculate the overall volume. The second approach dissects the cage's interior into distinct segments for individual volume assessments. The effectiveness of these methods was tested on a cage exposed to extreme wave and current conditions, followed by simulations to investigate optimal sensor configurations for precise volume determination. Among the evaluated methods, the *Cylinder with Cone* method is praised for its simplicity, whereas the *Signed Volume* and *Projection* methods emerge as the gold standard for accuracy. A pivotal finding is the imperative of sensor placement for precision in volume calculations, with an optimal configuration comprising four sensors on the rim and one at the bottom centre. For heightened precision, a distribution of sensors between the rim, bottom centre, and cage side is endorsed in tandem with the *Signed Volume* or *Projection* method.

1. Introduction

1.1. Background

Aquaculture cages, particularly for coldwater species like Atlantic salmon, play a pivotal role in global marine and coastal aquaculture. In 2020, Atlantic salmon alone constituted a significant 32.6% of all finfish species in marine and coastal aquaculture (FAO, 2022), underscoring the immense economic and ecological importance of these aquaculture systems. Predominantly, these setups involve net cages of the gravity type, characterized by a floating collar at the surface to maintain buoyancy and weights at the bottom to stretch the net.

In more exposed locations, where wave and current activity are prevalent, a sinker collar is often employed instead of single weights. The sinker collar's primary function is to ensure the net remains stretched downwards while it also contributes to maintaining the net's horizontal stretch. A significant challenge in these regions is the reduction of cage volume due to environmental forces, which has been

extensively documented in the literature (Aarsnes et al., 1990; Lader et al., 2003; Fredheim, 2005; Huang et al., 2006; Li et al., 2006; Huang et al., 2007; Zhao et al., 2007; Tsukrov et al., 2011; DeCew et al., 2013; Qu et al., 2019). This reduction in cage volume directly impacts farmed fish's welfare. A decrease in the available space can induce stress in the fish, leading to lower overall health and growth rates (Johannesen et al., 2021; Ortuño et al., 2001; Rowland et al., 2006; Harper and Wolf, 2009), and can escalate mortality rates (Turnbull et al., 2005).

Given the profound implications, it is crucial to investigate how wave and current exposure can lead to the shrinkage of cage volume. Therefore, it is essential to establish reliable methods for measuring the volume reduction. This includes knowledge of where and how to make the measurements and how to analyse the data.

In laboratory-scale models, markers can be attached to the net cage for this purpose, as suggested by Lader and Enerhaug (2005). In full-sized cages, methods such as acoustic markers (DeCew et al., 2013) or echo sounders (Kristmundsson et al., 2023) can be employed.

* Corresponding author at: Firum, við Áir 11, Hvalvík, FO 430, Faroe Islands.

E-mail address: hedin@firum.fo (H.I. Abrahamsen).

URLs: <https://www.firum.fo>, <https://www.setur.fo> (H.I. Abrahamsen).

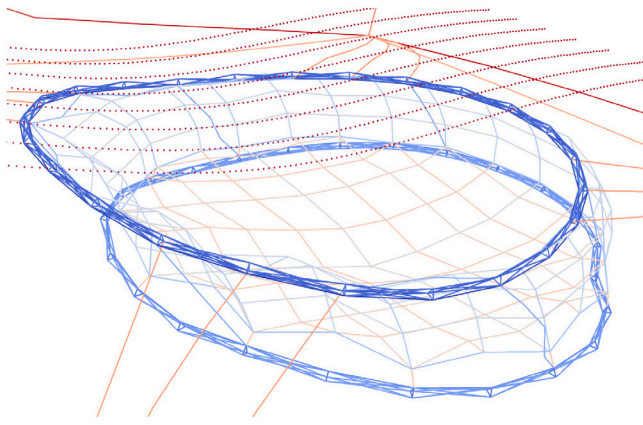


Fig. 1. Aquaculture cage deformation simulated with AquaFE (Tsukrov et al., 2003).

These techniques capture displacement in all three spatial dimensions, providing comprehensive insights into the cage dynamics under various environmental conditions. Similarly, a numerical model of the cage, depicted in Fig. 1, offers a full 3D view of the cage.

Acoustic markers, as used by DeCew et al. (2013), would require a substantial amount of receivers in a large sea cage (Klebert et al., 2015; Su et al., 2021) and echo sounders would require power requiring equipment that also may be vulnerable in harsh environments with high waves and strong currents. Our project was in an exposed area, and the cage had no power supply. A more straightforward and commonly employed method in full-sized net cages involves measuring the pressure at strategic points on the cage to determine the depth at these locations, providing data on vertical displacement, as discussed in studies by Lader et al. (2008) and Klebert et al. (2015). An example of such a measurement setup is illustrated in Fig. 2. To estimate horizontal displacement, it can be assumed that the entire net is stretched in the same direction. This solution does not require an external power supply and is very robust, as each sensor has its own battery and does not need to communicate to the outside world. When determining the shape of the net using pressure sensors, it is assumed that the water surface is flat.

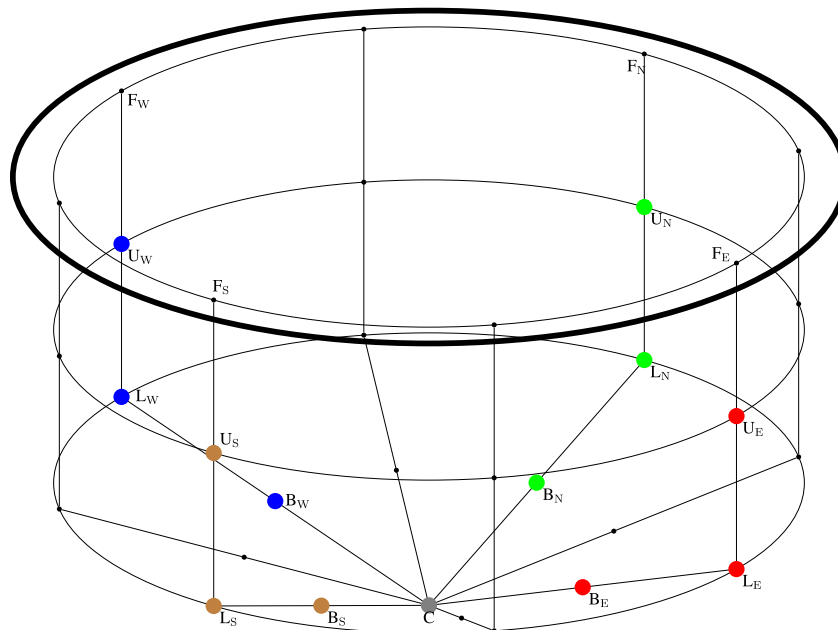


Fig. 2. Example of pressure sensors on a net cage: three sensors at each cardinal compass direction, with U midway between the water surface and bottom rim, L on the bottom rim, and B halfway between the bottom centre and rim. One sensor C is located at the bottom centre. F denote the floating collar.

In 2015, the aquaculture company MOWI initiated a pilot fish farming project in the bay of Sandsvåg, Faroe Islands. The local research station Firum equipped a cage with pressure tags and conducted measurements of waves and currents, as detailed by Abrahamsen and Patursson (2017). Building upon the results and experiments conducted in Sandsvåg, this study explores various methods for calculating the volume of cages. It establishes best practices for determining volume reduction in such settings.

1.2. Review of previous studies

Two main approaches have been employed in previous studies to calculate the volume in cages:

Surface Analysis: Examine the surface of the cage to derive its volume using *Divergence Theorem*.

Layered Division: Divide the cage's interior into layers, potentially subdividing each layer into sections. Calculate the volume of each division and sum them up.

Regarding the *Surface Analysis*, DeCew et al. (2013) had a relatively stiff sinker collar. They used three methods to calculate the volume, and two of these can be classified under the *Surface Analysis* approach, namely the *Divergence* method (Huang et al., 2007) and the *Signed Volume* method (Zhang and Chen, 2001).

Regarding the *Layer Division*, Lader et al. (2008) had a cage without a sinker collar. They assumed that the deformation of the net was in the direction of the current and that the net between the pressure sensors was stretched. They then calculated the volume of prisms formed by the pressure sensors in each two-depth layer and assumed the relative volume in the cage to be proportional to the relative volume in the prisms.

Klebert et al. (2015) employed the same approach, naming it the *Pancake* method. In their approach, each layer was approximated to a frustum. However, they found this assumption to be unsuitable in high deformation. As a result, they introduced the *Polygon* method. This method defined a plane parallel to the surface at each node. A polygon was positioned on each plane such that one of its corners was the node, while the other corners were determined through linear interpolation

of the neighbouring nodes. The volume was then calculated using Simpson's rule.

The *Scalar triple product* method that DeCew et al. (2013) employed can be classified under the Layered Division approach. The method was used by Huang et al. (2006) and has later been used by many others, including Mjåtveit et al. (2022), Chen et al. (2021), Dong et al. (2021). The total volume of the cage is divided into layers. Each of these layers is divided into circular sectors, and each circular sector is again divided into three tetrahedrons and a circle segment. The volume of each tetrahedron was calculated and added together. The circle segment was left out.

The study by Xu and Qin (2020) offers a comprehensive review of fluid–structure interactions within cage-based aquaculture systems. Their review includes “Cage deformation and volume reduction”, where they reexplain the *Scalar triple product*, the *Divergence*, the *Signed volume*, and the *Polygon* method.

1.3. Objective

The purpose of this study is to:

- Establish volume calculation methods that ensure accuracy even with significant cage deformation and can easily be implemented on a computer.
- Demonstrate a practical application of these methods using pressure sensors on a cage.
- Conduct simulations to ascertain the minimum number of sensors required for satisfactory accuracy in volume calculations of a cage.

1.4. Outline of the paper

This paper is organized into five main sections to present a comprehensive study of volume calculations in deformed aquaculture cages:

Section 2, ‘Methods’: This section details the methodologies used in this study, including data collection, the Surface Analysis approach, the Layered Division approach for volume calculation, the implemented calculation methods, and an examination of volume reduction.

Section 3, ‘Results’: Here, we present the findings of our study, focusing on the volume reduction observed in actual aquaculture cages and simulated models.

Section 4, ‘Discussion’: This part delves into a detailed discussion of the results. It includes an analysis of the number of sensors needed for accurate measurements, the effectiveness of different methods used for volume calculation, and the limitations of using pressure sensors in determining cage volume.

Section 5, ‘Summary and Conclusion’: This section recaps the examination and comparison of various methods for calculating the volume in aquaculture cages and determining the minimum number of sensors needed for accurate volume estimation. The section discusses the implementation and evaluation of the *Signed Volume* and *Polygon* methods, along with more straightforward techniques like *Cylinder with cone* method.

2. Methods

2.1. Data collections

The data in this study were collected from a cage at an aquaculture site owned by Mowi located at Sandsvåg in the Faroe Islands. Simulations were done of the same cage.

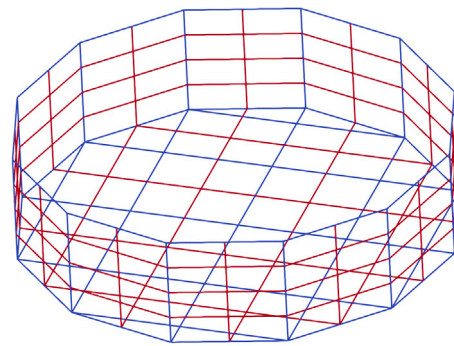


Fig. 3. The undisturbed cage from a simulation with AquaFE tool, showing the blue rope frame and the red net elements. After the deployment, the weight in the centre will form the bottom into a cone.

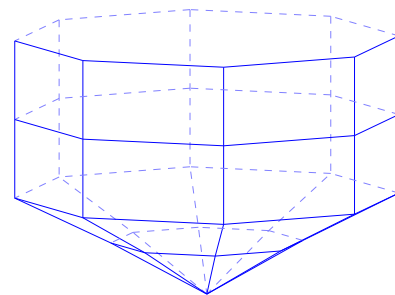


Fig. 4. The cage is simplified by drawing straight lines between sensors on the cage or between junctions of the frame in the simulated cage. The cage is depicted in solid blue lines when viewed from the outside and in light blue dashed lines when viewed from the inside.

The cage had a circumference of 120 m, and the depth from the floating collar to the sinker collar was 15 m. The weight of the sinker collar was around 85 kg m^{-1} . Equipment in the centre of the bottom weights around 300 kg. Two data sets were analysed: one from a calm day on 06 November 2016 and another from a stormy day on 20 December 2016, as referenced in Abrahamsen and Patursson (2017).

The data collected from the aquaculture site comprises measurements taken with pressure sensors placed on a cage, as illustrated in Fig. 2. The sensors located midway between the water surface and the bottom rim are marked U, those on the bottom rim are marked L, those halfway between the bottom centre and rim are marked B, and the sensor at the bottom centre is denoted C. Although the floating collar has no sensors, being at the water surface, it is included in the calculations and is indicated as F.

Model data were acquired by simulating the cage, depicted in Fig. 1, with the AquaFE tool, as referenced in Tsukrov et al. (2003). The simulated weather conditions were: wave height $H_{m0} = 4 \text{ m}$ with steepness of $\frac{1}{22}$ using a PM-spectrum, and a current speed of 30 cm s^{-1} . The undisturbed cage is depicted in Fig. 3. In this figure, the cage's frame is illustrated in blue and consists of rope elements. There are 12 vertical ropes positioned around the circumference of the cage. The net elements, shown in red, are integrated into this frame. For volume calculations, the space encompassed by the frame is considered. Consequently, all junctions involving the ropes are included in the volume calculation.

All the volume calculations build on simplifications of the cage. One simplification of the cage is shown in Fig. 4, where straight lines are drawn between sensors on the cage or between junctions of the frame in the simulated cage. Note that the simulated cage may have up to 12 junctions per layer, whereas the depicted simplification has eight.

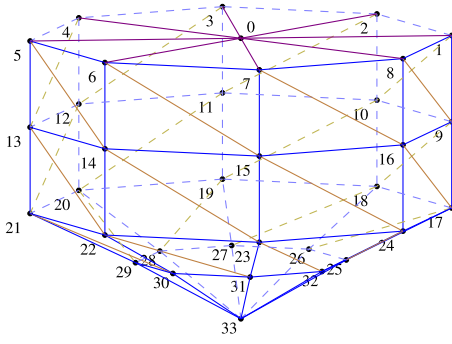


Fig. 5. The surface S of the cage from Fig. 4. S is divided into N triangles S_i to form a polyhedron.

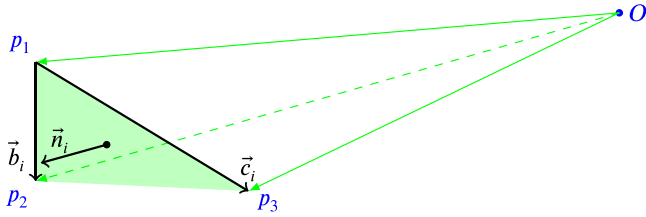


Fig. 6. Together with the origin O , the triangle S_i (shaded green) makes up a tetrahedron. The points p_1 , p_2 , and p_3 have to be chosen in clockwise order seen from the interior of the polyhedron, shown in Fig. 5, to get the normal vector \vec{n}_i to point out of the polyhedron.

2.2. Volume calculation using the surface analysis approach

In general, the volume of a 3D shape can be derived using the *Divergence Theorem*:

$$\iiint_V \vec{\nabla} \cdot \vec{f} dV = \iint_S \vec{f} \cdot \vec{n} dA \quad (1)$$

Where V is the volume enclosed by the surface S , \vec{n} is the normal vector pointing outward at every point on the surface, and \vec{f} is a continuously differentiable vector field in the region containing V . The surface S is assumed to be smooth or piecewise-smooth, allowing for the theorem to apply in cases where the surface can be broken down into a finite number of smooth surface pieces.

If \vec{f} is chosen such that $\vec{\nabla} \cdot \vec{f} = 1$, the triple integral on the left-hand side of Eq. (1) will yield the volume V .

To get a discrete version of Eq. (1), the surface S of the cage simplification in Fig. 4 is divided into triangles S_i as shown in Fig. 5, to ensure all surfaces are plan, and thus, the cage is simplified to a polyhedron. Eq. (1) can then be simplified for each face S_i as $V = \sum_{i=1}^N \iint_{S_i} \vec{f} \cdot \vec{n}_i dA$.

Choosing $\vec{f} = \frac{1}{3}[x \ y \ z]^T$ makes $\vec{\nabla} \cdot \vec{f} = 1$ and the dot product $\vec{f} \cdot \vec{n}_i$ constant over S_i , as shown in Appendix A.1. Thus $\vec{f} \cdot \vec{n}_i$ can be taken out of the integral and Eq. (1) becomes

$$V = \sum_{i=1}^N \vec{f} \cdot \vec{n}_i A_i$$

and if we let $\vec{a}_i \in S_i$, we can write:

$$V = \sum_{i=1}^N \frac{1}{3} \vec{a}_i \cdot \vec{n}_i A_i \quad (2)$$

Let \vec{b}_i and \vec{c}_i be two edges of S_i as shown in Fig. 6, such that the cross product $\vec{b}_i \times \vec{c}_i$ points out of the polyhedron, the normal vector \vec{n}_i and the area A_i of the surface S_i are respectively

$$\vec{n}_i = \frac{\vec{b}_i \times \vec{c}_i}{|\vec{b}_i \times \vec{c}_i|}, A_i = \frac{1}{2} |\vec{b}_i \times \vec{c}_i| \Rightarrow \vec{n}_i A_i = \frac{1}{2} (\vec{b}_i \times \vec{c}_i)$$

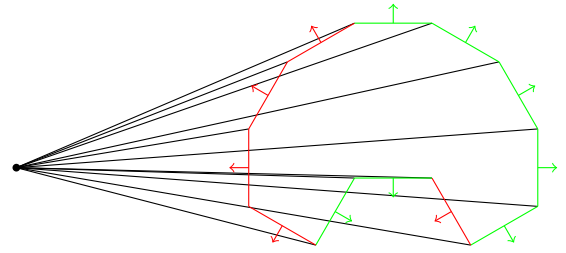


Fig. 7. A plan section through a polyhedron, simplifying it to a polygon, with surfaces S_i simplifying to lines. Negative triangles are shown with a red surface line, positive with a green.

and Eq. (2) expands to:

$$V = \sum_{i=1}^N \frac{1}{6} \vec{a}_i \cdot (\vec{b}_i \times \vec{c}_i)$$

which is the background for the *Divergence* method.

$\vec{a}_i \cdot (\vec{b}_i \times \vec{c}_i)$ is equivalent to the determinant $|\vec{a}_i \vec{b}_i \vec{c}_i|$, thus:

$$V = \sum_{i=1}^N \frac{1}{6} |\vec{a}_i \vec{b}_i \vec{c}_i| \quad (3)$$

which is the background for the *Signed volume* method.

Given the points p_1 , p_2 , and p_3 from Fig. 6, we get that $\vec{b}_i = \vec{p}_2 - \vec{p}_1$ and $\vec{c}_i = \vec{p}_3 - \vec{p}_1$ and choosing $\vec{a}_i = \vec{p}_1$ we can write determinant in Eq. (3) as¹:

$$\begin{aligned} |\vec{a}_i \vec{b}_i \vec{c}_i| &= |\vec{p}_1 \ \vec{p}_2 - \vec{p}_1 \ \vec{p}_3 - \vec{p}_1| \\ &= |\vec{p}_1 \ \vec{p}_2 \ \vec{p}_3| = |M_i| \end{aligned}$$

and the volume becomes

$$V = \frac{1}{6} \sum_{i=1}^N |M_i| \quad (4)$$

Fig. 7 shows a section through a polyhedron, simplifying it to a polygon, with surfaces S_i simplifying to lines. When all the normal vectors point out of the polygon, triangles with the origin and normal vector on the same side of the surface line are assigned a negative area and are shown with a red surface line. In contrast, triangles with the origin and normal vector on opposite sides of the surface line are assigned a positive area and are shown with a green surface line.

This principle extends to a polyhedron: when all the normal vectors of the surfaces S_i point out of the polyhedron, tetrahedrons with the origin and normal vector on the same side of the surface S_i have a negative volume, while those with the origin and normal vector on opposite sides have a positive volume. Summing all volumes, where some are negative and some positive, gives the polyhedron's volume. The location of the origin, whether inside or outside the polyhedron, does not affect the result. Similarly, the polyhedron does not need to be convex.

Another possibility for the choice of \vec{f} to get $\vec{\nabla} \cdot \vec{f} = 1$ is setting the first two components to zero, i.e. $\vec{f} = [0 \ 0 \ z]^T$. This choice simplifies the divergence to a constant value since $\vec{\nabla} \cdot \vec{f} = \partial_z z = 1$. With \hat{z}_i as the average height of a slanted prism with the surface triangle S_i as one end and its projection onto the xy -plane as the other, the formula for the volume of the simplified cage can be derived from divergent theorem, as shown in Appendix A.2, to be

$$V = \frac{1}{2} \sum_{i=1}^N (b_{ix}c_{iy} - b_{iy}c_{ix})\hat{z}_i. \quad (5)$$

¹ Adding one column to another column in a matrix does not change the determinant.

Similarly, choosing $\vec{f} = [x\ 0\ 0]^T$ and $\vec{f} = [0\ y\ 0]^T$ allows the volume to be expressed respectively as:

$$V = \frac{1}{2} \sum_{i=1}^N \hat{x}_i \cdot (b_{iy}c_{iz} - b_{iz}c_{iy}) \quad (6)$$

$$V = \frac{1}{2} \sum_{i=1}^N \hat{y}_i \cdot (b_{iz}c_{ix} - b_{ix}c_{iz}) \quad (7)$$

where the surface triangles S_i are projected on respectively the yz and xz plan multiplied by the distances from the plan to the respective geometrical centre of S_i .

Eq. (5) (6), and (7) have not been used in previous studies but are developed in this study. We name it the *Projection* method. The name can include which plan the surface is projected onto, e.g. *Projection onto the xy-plane*

2.3. Volume calculations using the layered division approach

A pyramid or cone consists of an arbitrarily shaped base connected to an apex. Its volume is:

$$V = \frac{1}{3} h A_b \quad (8)$$

One method in the *Layered Division* approach is dividing the total volume into frustums. In geometry, a frustum is a portion of a solid, usually a cone or pyramid, that lies between two parallel planes intersecting the solid (Wikipedia contributors, 2022). The volume of a frustum is given by:

$$V = \frac{1}{3} h_f (A_b + \sqrt{A_b A_t} + A_t)$$

where h_f is the perpendicular distance between the planes and A_b and A_t are the areas of the base and top planes, respectively.

The cross-sectional area of the frustum varies quadratically with height, satisfying the conditions for exact results using Simpson's rule. If a third plane A_m is placed midway between the two planes, the volume of the frustum can be calculated using Simpson's rule:

$$V = \frac{1}{6} h_f (A_b + A_t + 4A_m) \quad (9)$$

which is the background for the *Polygon* method.

If the cage has both a floating and a sinker collar, a more straightforward method is to calculate the cage as a cylinder. The volume can then be calculated as the cage's water surface area A multiplied by the perpendicular height h from the cage's bottom to the water surface:

$$V = hA \quad (10)$$

The average height can be used if the bottom rim is not parallel to the water surface. With a slanted bottom, the volume below the bottom rim can be calculated as a cone using Eq. (8).

2.4. Implemented calculation methods

Two systematic triangulations were used in this study: one depicted in Fig. 8, which is identical to that in Fig. 5, and another in Fig. 9, where the squares are divided the other way than in Fig. 8. Changing the triangulation changes the object and, thus, the volume. Notably, the top and the bottom centre serve as convergence nodes for every column, consistently depicted in every node in the first and last rows of Figs. 8 and 9.

The dataset used for analysis in this study has been deposited in the Zenodo repository and is accessible via the following DOI: 10.5281/zenodo.10202190. The methods are the *Signed Volume* method that uses Eq. (4), the *Projection onto the xy-plane* method that uses Eq. (5), the *Scalar triple product* method, the *Polygon* method that uses Eq. (9), the *Cylinder* method that uses Eq. (10), and the *Cylinder with Cone* method uses Eqs. (8) and (10).

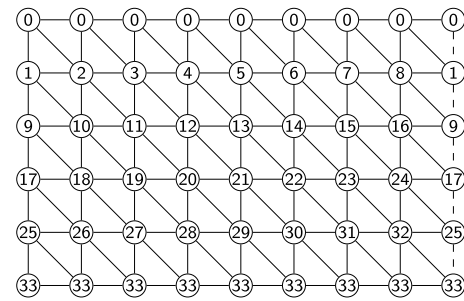


Fig. 8. The triangulation of the squares in the surface of the net. The numbers are the same as in Fig. 5.

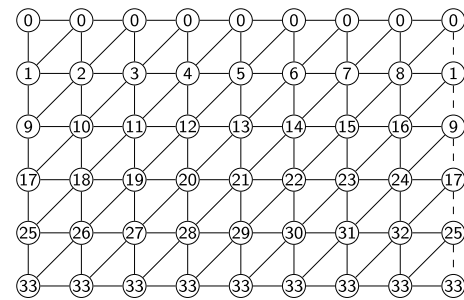


Fig. 9. The triangulation, when the squares are divided the other way than in Fig. 8.

Table 1

Overview of short names given combinations of methods and triangulations.

Short name	Method	Triangulation
SVa	<i>Signed Volume</i>	Fig. 8
SVb	<i>Signed Volume</i>	Fig. 9
Pol	<i>Polygone</i>	-
Cyl	<i>Cylinder</i>	-
Con	<i>Cylinder with Cone</i>	-

The *Signed Volume*, *Projection onto the xy-plane*, and *Scalar triple product* methods yield identical results when applied to the same object, such as the triangulations depicted in Figs. 8 and 9. Therefore, the *Signed Volume* method represents all three methods in the results.

The *Polygon*, the *Cylinder*, and *Cylinder with cone* methods do not utilize the triangulations depicted in Figs. 8 and 9, and do therefore not calculate on the same objects as the *Signed Volume* method and do therefore not necessarily give the same results.

A limitation of the *Polygone* method arises when a sensor is positioned above the layer it is intended to be beneath. This misplacement leads to a scenario where the layers cross each other, invalidating the assumptions underpinning Eq. (9), consequently causing the method to fail.

Each combination of method and triangulation has been given a short name, shown in Table 1, used in the results graphs.

2.5. Volume reduction

The relative volume is defined as the ratio between the volume of a cage and its undisturbed state. Let R denote the relative volume of the cage, and \hat{R} represent the relative volume of its simplification. It is assumed that \hat{R} is approximately equal to R , as expressed in Eq. (11):

$$R \approx \hat{R} = \frac{V}{V_0} \quad (11)$$

where V is the volume of the simplification, and V_0 is the volume of the cage in its undisturbed state.

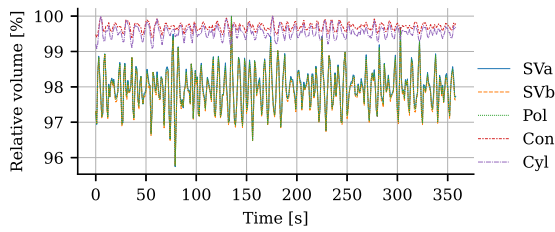


Fig. 10. Relative volume of each simplification in calm weather.

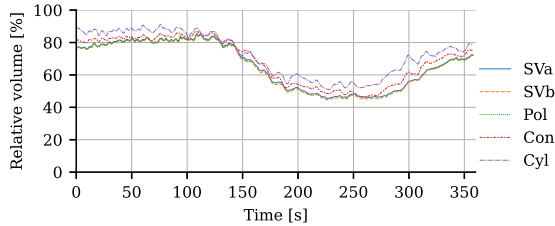


Fig. 11. Relative volume of each simplification in stormy weather.

In the aquaculture cage, the undisturbed volumes were obtained from the measurements on a calm day. For each method employed, the maximum volume observed this day served as V_0 to be used in Eq. (11).

In the simulated cage, the undisturbed volume used in Eq. (11) corresponds to the volume of the cage as depicted in Fig. 3.

2.6. Optimal sensor counts for volume estimation via simulations

In the full-size cage depicted in Fig. 2, sensor availability is limited, and these sensors only provide pressure data. These limitations make accurate volume estimation challenging. Conversely, in the simulated cage, the exact positions of all junctions are known, allowing for simulations that emulate placing sensors at selected junctions of an actual aquaculture cage.

We define *Layers* and the number of *Sensors* per layer for selection purposes. The *Layers* align with those shown in Fig. 2, and the combinations of layers in our calculations are labelled as *All*, *FULBC*, *FLBC*, *FULC*, *FLC*, *FUL*, and *FU*. The term *Sensors* denotes the number of junctions included in each layer, with options being 3, 4, 6, and 12 sensors. Notably, the centre-bottom junction is always singular.

We employ the *Signed Volume* method, referred to as “SVa”, using all 97 junctions to calculate what we consider the “true” volume reduction. Other sensor counts and methods are then compared against this baseline to evaluate their accuracy.

3. Results

3.1. Volume reduction in the aquaculture cage

Fig. 10 depicts the relative volume in calm weather. The results from the *Cylinder* and *Cylinder with Cone* methods exhibit smaller variations than the other methods. This is because the other methods account for the bulges in and out of the cage’s side and bottom, while the *Cylinder* and *Cylinder with Cone* methods exclude this effect.

The results from the *Signed Volume* method and the *Polygon* method are highly similar, with a maximum difference of 0.225 %-points.

Fig. 11 shows the cage’s relative volume on a stormy day. At the maximum volume reduction, the volume decreased to less than half its original size.

Fig. 12 illustrates the difference in relative volume between results from calculation with each method, and the results from calculation using the *Signed Volume* method on the triangulation shown in Fig. 8, labelled as “SVa”.

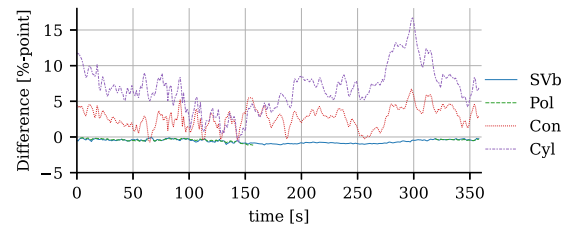


Fig. 12. Difference between relative volumes and relative volumes calculated with the *Signed Volume* method, R_{SVa} , in stormy weather.

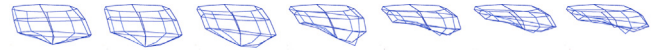


Fig. 13. The shape of a net, drawn from measured pressure data. There are 30 s between each drawing, and the total volume reduction after 180 s.

The *Signed Volume* “SVa” and *Polygon* methods, where it does not fail, produce almost indistinguishable volumes, with the maximum deviation around 1 %-point.

Fig. 13 sketches the cage movements, highlighting that significant deformations can elevate the bottom of the cage above the sinker collar. As pointed out in the text before Eq. (3), such uplift leads to the failure of the *Polygon* method. As depicted in Fig. 11, this limitation becomes evident in the first three measurements, as well as in the intervals of 65 s to 68 s, 144 s to 145 s, and 159 s to 319 s. The method’s inability is prevalent at large deformations.

3.2. Volume reduction in a simulated cage

Fig. 14(a) shows the relative volume reduction calculated using the *Signed Volume* method “SVa”. The plot headlines indicate which layer combination is utilized for the volume calculations. Within these plots, the lines represent the number of sensors per layer.

Fig. 14(b) depicts the difference in percentage points between the calculated volume reduction, using fewer junctions, and the “true” volume reduction, i.e. where all junctions are used in the calculations.

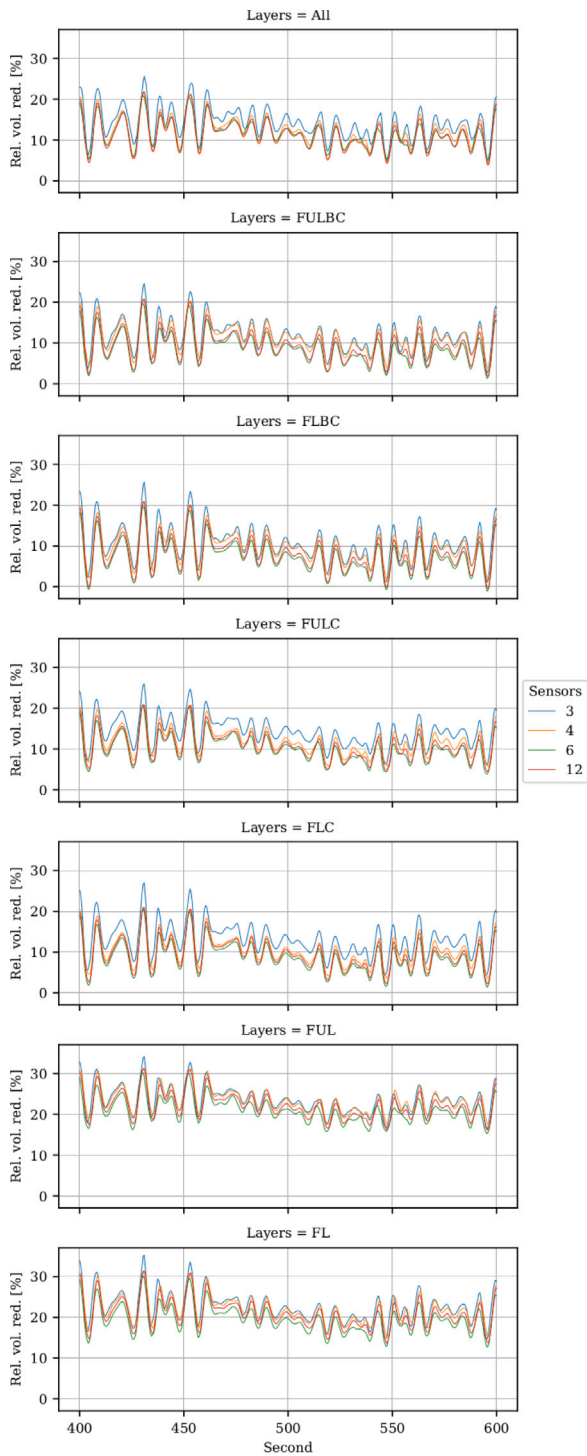
In the top panel of Figs. 14(a) and 14(b), calculations are presented where all layers are utilized. When employing 12 sensors in each layer, the difference (Figs. 14(b)) is inherently zero as it represents the “true” volume. However, using 6 or 4 sensors per layer results in an error margin of less than ± 1 pp (percentage point). With three sensors, the error ranges between +1 pp and +5 pp, indicating an overestimation in the volume reduction.

The layer combination *FULBC* is used in the subsequent panel, consistent with the measurements elaborated upon in Section 3.1. The configuration with 12 sensors per layer has a calculated reduction of approximately 2 pp lesser than the “true” value, that is, going from using all layers *FULBC* leads to an underestimation of the volume reduction.

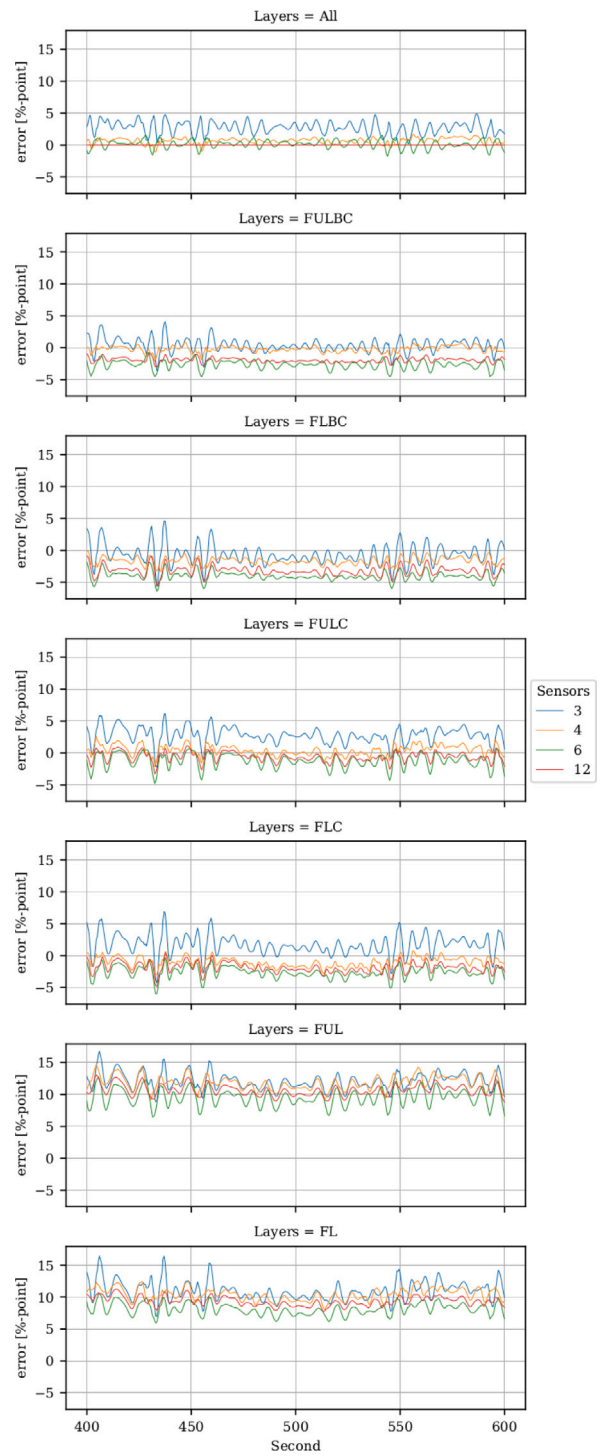
Interestingly, the overestimation of volume reduction using fewer sensors per layer and the underestimation, if you go from all layers to *FULBC*, that the configuration with four sensors per layer appears quite precisely with an error within ± 1 pp. However, the 3-sensor configuration deviates between ± 4 pp.

The results using the *Polygon* method are presented in Figs. 15(a) and 15(b). Only combinations that include the bottom centre, C, are employed in the *Polygon* method.

The *Cylinder* and *Cylinder with Cone* methods have no layer combinations as in the other methods. In the *Cylinder* method, the only sensors used are those on the bottom rim L, and in the *Cylinder with Cone* method, additionally the one in the bottom centre C. The results from this method are shown in Figs. 16(a) and 16(b).



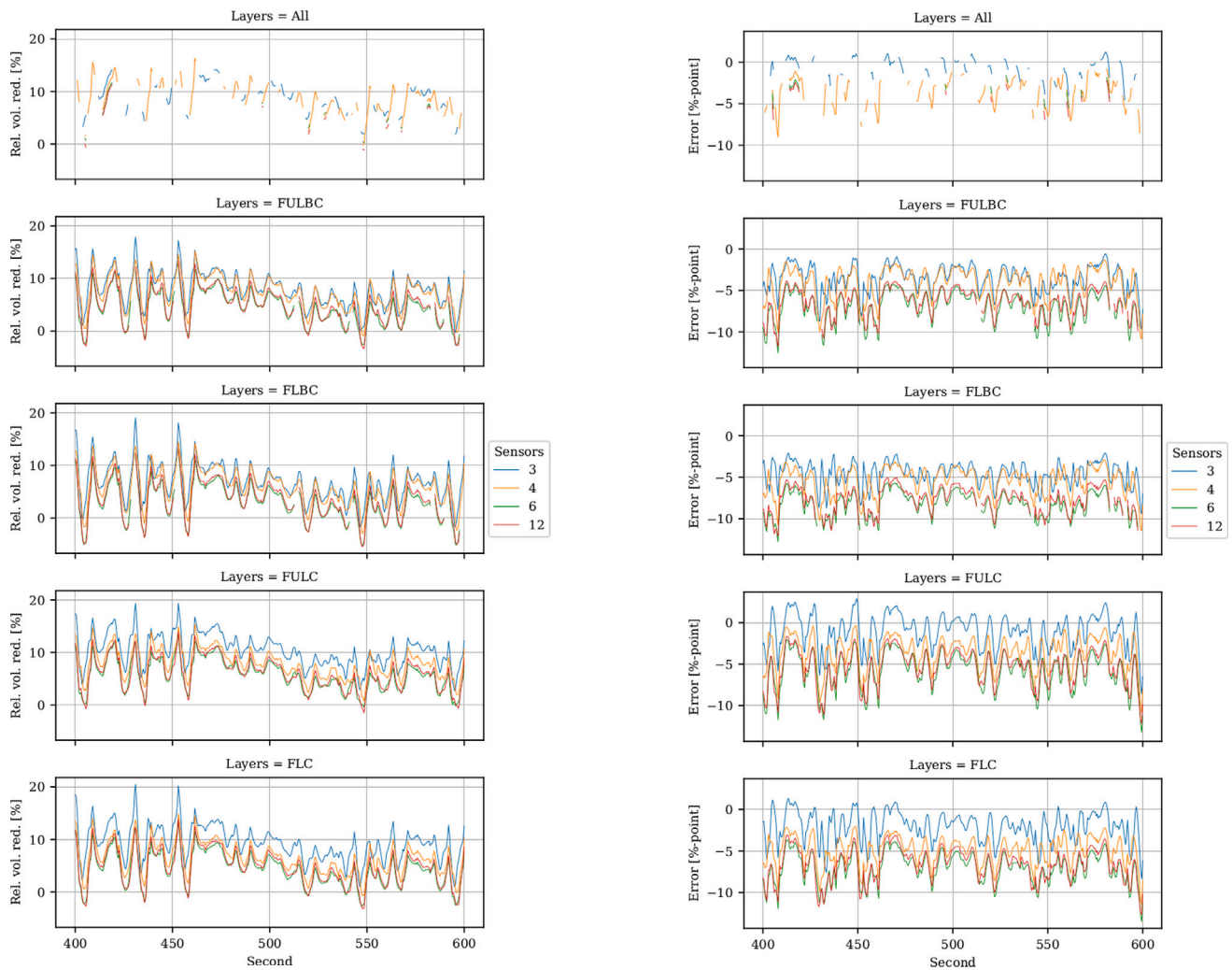
(a) Volume reduction calculations.



(b) Volume reduction calculation accuracy.

The difference between calculated volume reduction (Figure 14a) and the “true” volume reduction, i.e. all layers and 12 sensors per layer.

Fig. 14. Results from calculating the cage volume with the *Signed Volume* method ‘SvA’ using diverse sensor arrangements. Each panel has one combination of layers, and the line colour represents the number of sensors in each layer.



(a) Volume reduction calculations.

(b) Volume reduction calculation accuracy.

The difference between calculated volume reduction (Figure 15a) and the “true” volume reduction, i.e. all layers and 12 sensors per layer.

Fig. 15. Results from calculating the cage volume with the Polygon method using diverse sensor arrangements. Each panel has one combination of layers, and the line colour represents the number of sensors in each layer.

4. Discussion

4.1. Number of sensors needed

A simple sensor configuration. The most straightforward sensor setup involves using just one sensor on the bottom rim. This configuration is suitable in cages with flat bottoms when the sinker collar remains parallel to the floating collar, typically in conditions with minimal wave activity and volume changes. An additional sensor in the bottom centre is needed, with a slanted bottom and a significant volume below the bottom rim.

If additional sensors are used, placing them strategically, one on the bottom rim upstream of the current and another downstream, is beneficial. This positioning accounts for the current effect of lifting the sinker collar upstream and lowering it downstream.

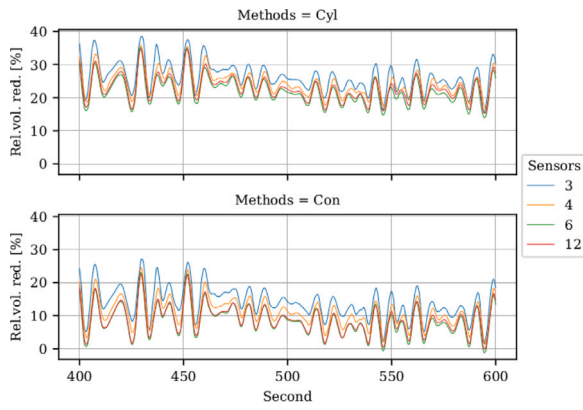
In scenarios where the direction of the current is unknown and the sinker collar’s alignment with the floating collar is unpredictable, at least three sensors are recommended.

Optimal sensor count per layer. Fig. 14(b) illustrates the error margin for different sensor counts. For a clearer comparison of sensor counts,

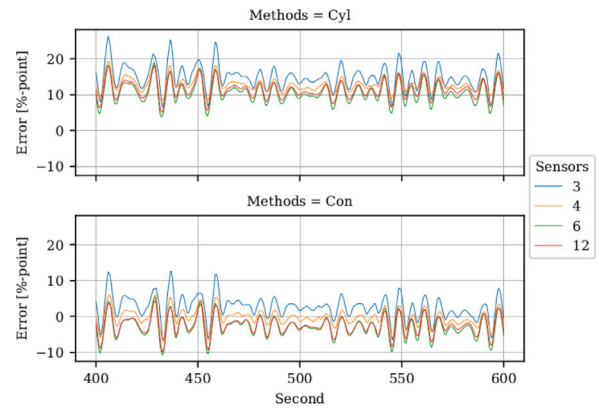
Fig. 17 is organized with one panel for each sensor count per layer, where the line colour denotes the layer combination.

The top panel of Fig. 17 reveals that using three sensors per layer results in a maximum error of approximately ± 7 pp (percentage points). Adding one sensor per layer, as shown in the second panel from the top, reduces the error to about ± 3 pp. Increasing the sensor count beyond this point does not significantly improve accuracy.

Layer considerations. The impact of different layer configurations on measurement accuracy can also be seen in Fig. 17. Notably, the second panel from the top shows that using four sensors per layer in the FLUBC configuration yields a minimal error of ± 1 pp. Omitting the U layer (FLBC) results in an underestimation of volume reduction, while omitting the B layer (FULC) leads to an overestimation. Interestingly, the FLC configuration, which omits both U and B layers, offers more balanced results compared to omitting just one of these layers. This trend is also observed in the top panel for configurations with three sensors per layer. In this setup, FLUBC shows the least error, FLBC tends to underestimate, FULC tends to overestimate, and FLC provides a middle ground.



(a) Volume reduction calculations.



(b) Volume reduction calculation accuracy.

The difference between calculated volume reduction (Figure 16a) and the “true” volume reduction, i.e. all layers and 12 sensors per layer.

Fig. 16. Results from calculating the cage volume with the *Cylinder* method and the *Cylinder with Cone* method using diverse sensor arrangements. Each panel has one combination of layers, and the line colour represents the number of sensors in each layer.

Recommendations. Based on our findings, we recommend the *FLC* layer configuration with four sensors per layer for general applications. This arrangement entails placing four sensors around the rim and one at the centre of the bottom. Alternatively, using three sensors on the bottom rim is also effective, or two sensors can suffice if the current direction is known.

For scenarios requiring heightened precision, increasing the number of sensors along each of the four sensor columns is advisable: one or two sensors on the side between the floating and sinker collar and one or two sensors between the bottom centre and rim.

4.2. Method to use

After determining the optimal sensor placement on the cage, the next question is which method to use in calculating the volume.

Fig. 18 displays each method’s percentage point error with three and four sensors on the bottom rim. With four sensors on the bottom rim, the *Signed Volume* method exhibits the slightest error, followed by the *Cylinder with Cone* method, with the *Polygone* method showing the highest error. The *Polygone* method underestimates the volume reduction, and the *Cylinder with Cone* overestimates it, though to a lesser degree.

When pursuing greater precision in the measurements, with sensors positioned on both the side of the cage, *U* in Fig. 2, and the bottom, *B* in Fig. 2, either *Polygone* or the *Signed Volume* method must be utilized. As already mentioned in the text before Eq. (3), the *Polygone* method may fail in large cage deformations. Under such conditions, the more dependable choice is the *Signed Volume* or *Projection* method.

4.3. Limitations in using pressure sensors in determining cage volume

This study used pressure sensors to determine the depth. This approach uses a system with a flat water surface and only static pressure. But dynamic pressure is also present in an environment with waves and currents.

The total pressure is according to the Bernoulli’s equation

$$p_t = p_d + p_s = \frac{1}{2} \rho v^2 + \rho g d$$

where p_t is the total pressure,² p_d the dynamic pressure, p_s the static pressure, ρ the density, v the velocity, g the gravity acceleration, and d is the depth.

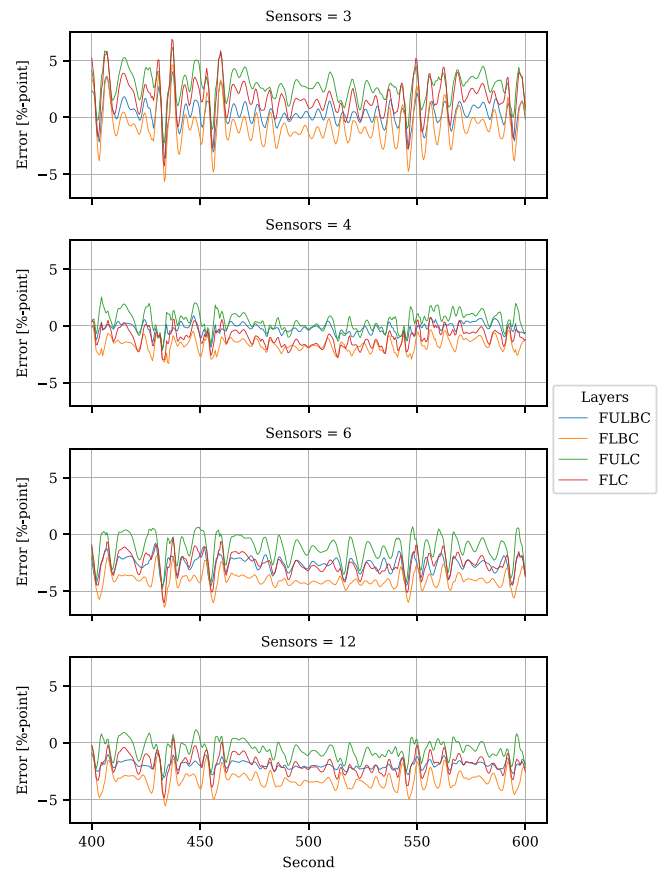


Fig. 17. The error in pp for *Layers* calculated using the “SVa” method. One plot per sensor count per layer and line colour represents the layer combination.

This shows that the static pressure is dependent on the depth, but the dynamic pressure is not and has to be eliminated to get the depth.

The dynamic pressure is due to the current speed and the speed of the particles inside the waves.

Locations with current speeds larger than the critical swimming speed of the fish will harm it and can, therefore, not be used for aquaculture. Hvas et al. (2019) estimated critical swimming speed for

² In this paper, all pressures are pressures over atmospheric pressure.

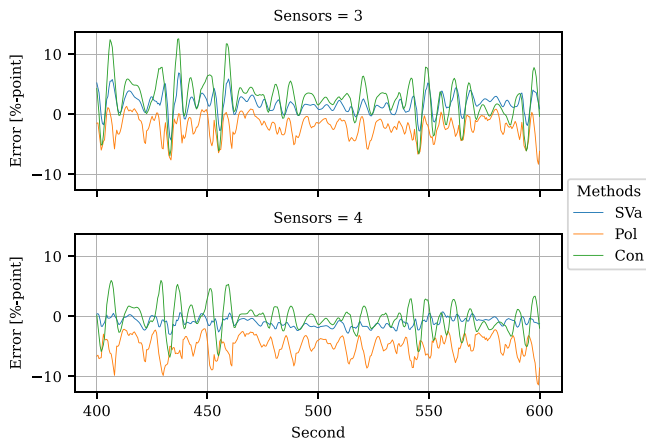


Fig. 18. The error in pp in the three methods: the *Signed Volume* method “SVa”, the *Polygon* method Pol, and the *Cylinder with Cone* method Con in a FLC configuration with three and four sensors on the bottom rim, respectively.

Atlantic salmon. They found that the fastest swimmers have critical swimming speeds up towards 1.1 m s^{-1} . The current speed is therefore limited to

$$v_c \leq 1.1 \text{ m s}^{-1}$$

The wave height will be limited even at very exposed locations because otherwise, it would harm the fish. This subject is not well researched (Hvas et al., 2021), but when setting the wave height H_{m0} to four meters, the maximum height H will be around eight meters. With a steepness ξ of one-tenth, the wavelength will be 80 m. The period will be

$$T = \sqrt{\frac{2\pi\lambda}{g}} = \sqrt{\frac{2\pi \cdot 80}{9.81}} = 7.2 \text{ s}$$

For this wave, the speed v_w of the particles inside the wave is limited to

$$v_w = \frac{H \cdot \pi}{T} \leq \frac{8 \cdot \pi}{7.16} = 3.5 \text{ m s}^{-1}$$

The combined speed v of the water from both current and waves is, therefore limited to

$$v = v_c + v_w \leq 1.1 + 3.5 = 4.6 \text{ m s}^{-1}$$

and the dynamic pressure p_d will be limited to

$$p_d = \frac{1}{2}\rho v^2 \leq \frac{1}{2}\rho 4.6^2 = \rho 11 \text{ m}^2 \text{ s}^{-2}$$

This dynamic pressure is equivalent to a depth d_d of

$$d_d = \frac{p_d}{\rho g} = \frac{11}{9.81} = 1.1 \text{ m}$$

The dept d to a pressure sensor is calculated with the formula:

$$d = \frac{p_s}{\rho g} = \frac{p_t - p_d}{\rho g} = d_m - d_d \leq \frac{p_t}{\rho g}$$

where d_m is the depth calculated from the measured pressure at the sensor. If the pressure sensors measure the total pressure, the depth of the sensor is less than calculated by ignoring the dynamic pressure, max 1.1 m less in the circumstances above. However, the dynamic pressure is not constant, so with the sensor at a constant distance from the surface, the calculated depth can show anything from this depth to a dept 1.1 m deeper.

5. Summary and conclusion

The primary objective of this study was to examine and compare various methods for calculating the volume in aquaculture cages, with

a secondary objective of determining the minimum number of pressure sensors required for adequate volume estimation.

A comprehensive review of previous studies identified two primary approaches to volume calculation in aquaculture cages. The first approach involves dividing the cage’s surface into triangular sections and then calculating the volume based on these triangles. The second approach divides the cage’s interior into smaller segments, with the volume of each segment being calculated separately.

In this study, we implemented the *Signed Volume* and the *Projection onto the xy-plane* method representing the first approach, and the *Scalar triple product* and *Polygon* methods, embodying the second approach. Our analyses focused on evaluating and comparing the efficacy of these two methods under various conditions.

The *Projection onto the xy-plane* is derived in this study and may be perceived by some as more straightforward. Additionally, we explored simpler volume calculation techniques like the *Cylinder Method* and the *Cylinder with Cone* method. The *Cylinder* method approximates the cage volume by multiplying its plan area with its height, while the *Cylinder with Cone* method includes the downward sloping of the cage bottom modelled as a cone. These methods, noted for their minimal sensor requirements, offer practical benefits in resource-limited scenarios.

These methods were tested on a full-size aquaculture cage under high waves and strong currents. While more straightforward, the *Cylinder with Cone* method did not match the accuracy of the *Signed Volume* method. However, the *Polygon* method showed an inherent limitation: it becomes inapplicable when significant deformations cause a sensor in a lower layer to surpass one in an upper layer.

Our findings also underline the importance of sensor placement. Using three sensors per layer is crucial in scenarios with unknown current directions. Simulations indicate that increasing to four sensors per layer enhances accuracy, but adding more than four sensors yields no significant improvement. Optimally, placing three or four sensors on the bottom rim and one in the bottom centre and employing the *Cylinder with Cone* method for calculation appears most effective. For heightened precision, we recommend distributing sensors between the rim and the centre of the bottom and on the side of the cage, employing the *Signed Volume* or *Projection* method.

In conclusion, this study compares volume calculation methods in aquaculture cages, highlighting the balance between accuracy and practical sensor deployment. Our recommendations offer guidance for optimal sensor placement and calculation method selection.

CRedit authorship contribution statement

Heðin I. Abrahamsen: Writing – original draft, Visualization, Validation, Methodology, Funding acquisition, Formal analysis, Conceptualization. **Tróndur T. Johannesen:** Writing – review & editing, Validation, Software, Formal analysis. **Óystein Patursson:** Writing – review & editing, Supervision. **Knud Simonsen:** Writing – review & editing, Supervision.

Declaration of competing interest

The authors declare that they have no known competing financial interests or personal relationships that could have appeared to influence the work reported in this paper.

Data availability

We have shared the link to our data/code at <https://doi.org/10.5281/zenodo.10202190>.

Declaration of Generative AI and AI-assisted technologies in the writing process

During the preparation of this work, the author(s) used Grammarly and Chat.GPT in order to improve the readability and language. After using this tool/service, the author(s) reviewed and edited the content as needed and take(s) full responsibility for the content of the publication.

Acknowledgements

We thank the company, Mowi, for allowing us to use the data.

Thanks, Gunnvør á Norði and Tróndur J. Kragesteen, Firum, for being PhD supervisors of the industrial part, Robert McCall, Deltares, for being the external supervisor, Bárður Joensen, University of the Faroe Islands, for advice, review and editing, and Erna Lava Olsen for providing language help, writing assistance or proofreading the article.

Funding

This study was financially supported by Firum, Innovations Fund Denmark, Betri Stuðul, Føroyagrúnnurin frá 1971, and Mowi.

Appendix. Choice of f in the divergence method

This appendix refers to Section 2.2 and examines functions \vec{f} where $\vec{\nabla} \cdot \vec{f} = 1$. Under these conditions, the left-hand side of Eq. (1), representing the Divergence Theorem, yields the volume of the polyhedra. The surface S_i is depicted in Fig. 6.

A.1. When f is set to $\frac{1}{3}[x y z]^T$

Let \vec{n} be a normal vector to S_i , and $f(\vec{x}) = \frac{1}{3}\vec{x}$. Then

$$\forall \vec{x} \in S_i \quad \vec{f}(\vec{x}) \cdot \vec{n} = c$$

where c is a constant.

Let $\vec{x}_1, \vec{x}_2 \in S_i$

$$\begin{aligned} & \vec{f}(\vec{x}_1) \cdot \vec{n}_i - \vec{f}(\vec{x}_2) \cdot \vec{n}_i \\ &= \frac{1}{3}(\vec{x}_1 - \vec{x}_2) \cdot \vec{n}_i \\ &= \frac{1}{3}\vec{x}_3 \cdot \vec{n}_i \end{aligned}$$

where \vec{x}_3 is parallel to S_i and thus orthogonal to n_i .

$$\begin{aligned} & \vec{f}(\vec{x}_1) \cdot \vec{n}_i - \vec{f}(\vec{x}_2) \cdot \vec{n}_i = 0 \\ \Rightarrow & \vec{f}(\vec{x}_1) \cdot \vec{n} = \vec{f}(\vec{x}_2) \cdot \vec{n} \quad \blacksquare \end{aligned}$$

A.2. When f is set to $[0 0 z]^T$

When f is set to $[0 0 z]^T$ the polyhedra described in Section 2.2 has volume

$$V = \frac{1}{2} \sum_{i=0}^N (b_{ix}c_{iy} - b_{iy}c_{ix}) \hat{z}_i$$

Where \vec{b}_i, \vec{c}_i are as described in Fig. 6, and \hat{z}_i is z-component of the centre of mass of S_i .

So the right-hand side of *Divergence theorem* becomes

$$\begin{aligned} V &= \iint_S \vec{f} \cdot \vec{n} dA \\ &= \sum_{i=0}^N \iint_{S_i} \vec{f} \cdot \vec{n}_i dA. \end{aligned}$$

Only looking at one term, and using $\vec{b}_i = p_2 - p_1$ and $\vec{c}_i = p_3 - p_1$, we get

$$S_i = \left\{ p_1 + \beta \vec{b}_i + \gamma \vec{c}_i \in \mathbb{R}^3 \mid 0 \leq \beta \leq 1 \wedge 0 \leq \gamma \leq \beta - 1 \right\}.$$

And integrating

$$\begin{aligned} & \iint_{S_i} \vec{f} \cdot \vec{n}_i dA \\ &= \int_0^1 \left[\int_0^{1-\beta} \vec{f}(\vec{p}_1 + \beta \vec{b}_i + \gamma \vec{c}_i) \cdot \frac{\vec{b}_i \times \vec{c}_i}{|\vec{b}_i \times \vec{c}_i|} \left| \vec{b}_i \times \vec{c}_i \right| d\gamma \right] d\beta \\ &= (\vec{b}_i \times \vec{c}_i)_z \int_0^1 \left[\int_0^{1-\beta} p_{1,z} + \beta b_{iz} + \gamma c_{iz} d\gamma \right] d\beta \\ &= (\vec{b}_i \times \vec{c}_i)_z \int_0^1 \left[\gamma p_{1,z} + \gamma \beta b_{iz} + \frac{1}{2} \gamma^2 c_{iz} \right]_{\gamma=0}^{1-\beta} d\beta \\ &= (\vec{b}_i \times \vec{c}_i)_z \int_0^1 (1-\beta) p_{1,z} + (\beta - \beta^2) b_{iz} + \frac{1}{2} (1-\beta)^2 c_{iz} d\beta \\ &= (\vec{b}_i \times \vec{c}_i)_z \left[\left(\beta - \frac{1}{2} \beta^2 \right) p_{1,z} + \left(\frac{1}{2} \beta^2 - \frac{1}{3} \beta^3 \right) b_{iz} \right. \\ & \quad \left. + \frac{1}{2} \left(\beta - \beta^2 + \frac{1}{3} \beta^3 \right) c_{iz} \right]_0^1 \\ &= (b_{ix}c_{iy} - b_{iy}c_{ix}) \left(\frac{1}{2} p_{1,z} + \frac{1}{6} b_{iz} + \frac{1}{6} c_{iz} \right) \\ &= \frac{1}{2} (b_{ix}c_{iy} - b_{iy}c_{ix}) \left(\frac{1}{3} p_{1,z} + \frac{1}{3} p_{2,z} + \frac{1}{3} p_{3,z} \right) \\ &= \frac{1}{2} (b_{ix}c_{iy} - b_{iy}c_{ix}) \hat{z}_i. \end{aligned}$$

And when we set it all together, we have

$$V = \frac{1}{2} \sum_{i=0}^N (b_{ix}c_{iy} - b_{iy}c_{ix}) \hat{z}_i. \quad \blacksquare$$

References

- Aarsnes, J., Rudi, H., Løland, G., 1990. Current forces on cage, net deflection. In: *Engineering for Offshore Fish Farming*. Thomas Telford Publishing, pp. 137–152.
- Abrahamsen, H., Patursson, Ø., 2017. Description of measurements on the aquaculture site sandsvág. In: *Fiskaaling rit. Technical Report 2017:03, P/F Fiskaaling (Aquaculture Research Station of the Faroes), viðÁir 11, FO-430 Hvalvík, Faroe Islands*.
- Chen, D., Wang, C., Zhang, H., 2021. Examination of net volume reduction of gravity-type open-net fish cages under sea currents. *Aquacult. Eng.* 92, 102128. <http://dx.doi.org/10.1016/j.aquaeng.2020.102128>, URL: <https://www.sciencedirect.com/science/article/pii/S0144860920301746>.
- DeCew, J., Fredriksson, D., Lader, P., Chambers, M., Howell, W., Osenki, M., Celikkol, B., Frank, K., Høy, E., 2013. Field measurements of cage deformation using acoustic sensors. *Aquacult. Eng.* 57, 114–125. <http://dx.doi.org/10.1016/j.aquaeng.2013.09.006>, URL: <http://www.sciencedirect.com/science/article/pii/S0144860913000903>.
- Dong, S., You, X., Hu, F., 2021. Experimental investigation on the fluid–structure interaction of a flexible net cage used to farm Pacific bluefin tuna (*Thunnus orientalis*). *Ocean Eng.* 226, 108872. <http://dx.doi.org/10.1016/j.oceaneng.2021.108872>, URL: <https://www.sciencedirect.com/science/article/pii/S0029801821003073>.
- FAO, 2022. The state of world Fisheries and aquaculture 2022. Towards blue transformation. FAO.
- Fredheim, A., 2005. Current Forces on Net Structures (Ph.D. thesis). NTNU Department of Marine Technology, Faculty of Engineering Science and Technology. Trondheim, Norwegian University of Science and Technology, Doctoral theses at NTNU, 2005:64.
- Harper, C., Wolf, J.C., 2009. Morphologic Effects of the Stress Response in Fish. *ILAR J.* 50 (4), 387–396. <http://dx.doi.org/10.1093/ilar.50.4.387>.
- Huang, C.C., Tang, H.J., Liu, J.Y., 2006. Dynamical analysis of net cage structures for marine aquaculture: Numerical simulation and model testing. *Aquacult. Eng.* 35 (3), 258–270. <http://dx.doi.org/10.1016/j.aquaeng.2006.03.003>, URL: <http://www.sciencedirect.com/science/article/pii/S014486090600029X>.
- Huang, C.C., Tang, H.J., Liu, J.Y., 2007. Modeling volume deformation in gravity-type cages with distributed bottom weights or a rigid tube-sinker. *Aquacult. Eng.* 37 (2), 144–157. <http://dx.doi.org/10.1016/j.aquaeng.2007.04.003>, URL: <http://www.sciencedirect.com/science/article/pii/S0144860907000416>.
- Hvas, M., Folkedal, O., Oppedal, F., 2019. Havbasert oppdrett - hvor mye vannstrøm tåler laks og rensefisk? - fiskevelferd og grenseverdier. In: *Rapport fra havforskningen. Technical Report 2019–37, Havforskningsinstituttet/Forskningsrådet, Trondheim, Norge*.

- Hvas, M., Folkedal, O., Oppedal, F., 2021. Fish welfare in offshore salmon aquaculture. *Rev. Aquacult.* 13 (2), 836–852. <http://dx.doi.org/10.1111/raq.12501>, URL: <https://onlinelibrary.wiley.com/doi/abs/10.1111/raq.12501>.
- Johannesen, Á., Patursson, Ø., Kristmundsson, J., Pætúrsonur Dam, S., Mulelid, M., Klebert, P., 2021. Waves and currents decrease the available space in a salmon cage. *bioRxiv* <http://dx.doi.org/10.1101/2021.07.23.453560>, URL: <https://www.biorxiv.org/content/early/2021/10/22/2021.07.23.453560>.
- Klebert, P., Patursson, Ø., Endresen, P.C., Rundtop, P., Birkevold, J., Rasmussen, H.W., 2015. Three-dimensional deformation of a large circular flexible sea cage in high currents: Field experiment and modeling. *Ocean Eng.* 104, 511–520. <http://dx.doi.org/10.1016/j.oceaneng.2015.04.045>, URL: <http://www.sciencedirect.com/science/article/pii/S0029801815001262>.
- Kristmundsson, J., Patursson, Ø., Potter, J., Xin, Q., 2023. Fish monitoring in aquaculture using multibeam echosounders and machine learning. *IEEE Access* 11, 108306–108316. <http://dx.doi.org/10.1109/ACCESS.2023.3320949>.
- Lader, P., Dempster, T., Fredheim, A., Jensen, Ø., 2008. Current induced net deformations in full-scale sea-cages for atlantic salmon (*Salmo salar*). *Aquacult. Eng.* 38 (1), 52–65. <http://dx.doi.org/10.1016/j.aquaeng.2007.11.001>, URL: <http://www.sciencedirect.com/science/article/pii/S0144860907000957>.
- Lader, P., Enerhaug, B., 2005. Experimental investigation of forces and geometry of a net cage in uniform flow. *IEEE J. Ocean. Eng.* 30 (1), 79–84. <http://dx.doi.org/10.1109/JOE.2004.841390>.
- Lader, P.F., Enerhaug, B., Fredheim, A., Krokstad, J., 2003. Modelling of 3D net structures exposed to waves and current. In: 3rd International Conference on Hydroelasticity in Marine Technology. Department of Engineering Science, The University of Oxford Oxford, UK, pp. 19–26.
- Li, Y.C., Zhao, Y.P., Gui, F.K., Teng, B., 2006. Numerical simulation of the hydrodynamic behaviour of submerged plane nets in current. *Ocean Eng.* 33 (17–18), 2352–2368.
- Mjåtveit, M.A., Cheng, H., Ong, M.C., Lee, J., 2022. Comparative study of circular and square gravity-based fish cages with different dimensions under pure current conditions. *Aquacult. Eng.* 96, 102223. <http://dx.doi.org/10.1016/j.aquaeng.2021.102223>, URL: <https://www.sciencedirect.com/science/article/pii/S0144860921000790>.
- Ortuño, J., Esteban, M., Meseguer, J., 2001. Effects of short-term crowding stress on the gilthead seabream (*sparus aurata* L.) innate immune response. *Fish & Shellfish Immunol.* 11 (2), 187–197. <http://dx.doi.org/10.1006/fsim.2000.0304>, URL: <https://www.sciencedirect.com/science/article/pii/S1050464800903048>.
- Qu, X., Hu, F., Kumazawa, T., Takeuchi, Y., Dong, S., Shiode, D., Tokai, T., 2019. Deformation and drag force of model square fish cages in a uniform flow. *Ocean Eng.* 171, 619–624. <http://dx.doi.org/10.1016/j.oceaneng.2018.12.016>, URL: <https://www.sciencedirect.com/science/article/pii/S0029801818306486>.
- Rowland, S.J., Mifsud, C., Nixon, M., Boyd, P., 2006. Effects of stocking density on the performance of the Australian freshwater silver perch (*Bidyanus bidyanus*) in cages. *Aquaculture* 253 (1), 301–308. <http://dx.doi.org/10.1016/j.aquaculture.2005.04.049>, URL: <https://www.sciencedirect.com/science/article/pii/S0044848605003030>.
- Su, B., Kelasidi, E., Frank, K., Haugen, J., Føre, M., Pedersen, M.O., 2021. An integrated approach for monitoring structural deformation of aquaculture net cages. *Ocean Eng.* 219, 108424. <http://dx.doi.org/10.1016/j.oceaneng.2020.108424>, URL: <https://www.sciencedirect.com/science/article/pii/S0029801820313317>.
- Tsukrov, I., Drach, A., DeCew, J., Robinson Swift, M., Celikkol, B., 2011. Characterization of geometry and normal drag coefficients of copper nets. *Ocean Eng.* 38 (17), 1979–1988. <http://dx.doi.org/10.1016/j.oceaneng.2011.09.019>, URL: <https://www.sciencedirect.com/science/article/pii/S0029801811002137>.
- Tsukrov, I., Eroshkin, O., Fredriksson, D., Swift, M., Celikkol, B., 2003. Finite element modeling of net panels using a consistent net element. *Ocean Eng.* 30 (2), 251–270. [http://dx.doi.org/10.1016/S0029-8018\(02\)00021-5](http://dx.doi.org/10.1016/S0029-8018(02)00021-5), URL: <http://www.sciencedirect.com/science/article/pii/S0029801802000215>.
- Turnbull, J., Bell, A., Adams, C., Bron, J., Huntingford, F., 2005. Stocking density and welfare of cage farmed atlantic salmon: application of a multivariate analysis. *Aquaculture* 243 (1), 121–132. <http://dx.doi.org/10.1016/j.aquaculture.2004.09.022>, URL: <https://www.sciencedirect.com/science/article/pii/S0044848604005538>.
- Wikipedia contributors, 2022. Frustum — Wikipedia, The Free Encyclopedia. URL: <https://en.wikipedia.org/w/index.php?title=Frustum&oldid=1130465453>. (Online; Accessed 9 January 2023).
- Xu, Z., Qin, H., 2020. Fluid-structure interactions of cage based aquaculture: From structures to organisms. *Ocean Eng.* 217, 107961. <http://dx.doi.org/10.1016/j.oceaneng.2020.107961>, URL: <https://www.sciencedirect.com/science/article/pii/S0029801820309136>.
- Zhang, C., Chen, T., 2001. Efficient feature extraction for 2D/3D objects in mesh representation. In: Proceedings 2001 International Conference on Image Processing (Cat. No.01CH37205), Vol. 3. pp. 935–938. <http://dx.doi.org/10.1109/ICIP.2001.958278>.
- Zhao, Y.P., Li, Y.C., Dong, G.H., Gui, F.K., Teng, B., 2007. Numerical simulation of the effects of structure size ratio and mesh type on three-dimensional deformation of the fishing-net gravity cage in current. *Aquacult. Eng.* 36 (3), 285–301. <http://dx.doi.org/10.1016/j.aquaeng.2007.01.003>, URL: <https://www.sciencedirect.com/science/article/pii/S0144860907000027>.